Received: 12 August 2024 | Revised: 14 November 2024 | Accepted: 16 November 2024

https://doi.org/10.56946/jce.v3i2.503

Journal of Chemistry and Environment

Research Article

Green Synthesis And Photoluminesce Study Of Dy Doped $CaCO_3$

Muhammad Bilal[1], Majid Ali[2*], Hammad Haider[2], Salman Ahmad[3], Saeed Anwar[3], Muhammad Jamshed[1,4*]

[1]Department of Chemistry, Kohat University of Science and Technology, Kohat-26000-Khyber Pakhtunkhwa, Pakistan.
[2]Department of Physics, Kohat University of Science and Technology, Kohat-26000-Khyber Pakhtunkhwa, Pakistan.
[2]Department of Chemistry, Abdul Wali Khan University, Mardan-23200, Khyber Pakhtunkhwa, Pakistan.
[4]School of Chemistry, and Xi'an Key Laboratory of Sustainable Energy Materials Chemistry, Xi'an Jiao Tong University, Xi'an 710049, P. R. China.
*Correspondence:
(Majid Ali) majidali58352@gmail.com,
(Muhammad Jamshed) muhammadjamshed@stu.xjtu.edu.cn

Abstract

In this study, we used water-soluble polysaccharides from melon to develop a new green method for the biological production of calcium carbonate crystals. SEM, FT-IR spectroscopy, and X-ray powder diffractometry were used to examine the resulting crystals. The host material is prepared with the amount of 5.549gm $CaCl_2$ and 5.2994gm Na_2CO_3. In the sintering process, the sample is subjected to its melting temperature in a furnace and then cooled evenly. The phosphor $CaCO_3$ is doped with differing proportions of Dy and SEM micrographs validate the material's nanostructure, which is essential for luminescence. By Dy doping with $CaCO_3$, then crystal structure of a molecule shows prominent XRD peaks. In UV photoluminescence spectra, the greatest emission peak is at 578nm while slake curve shows that for 3 mol% Dy concentrations, show higher luminescence intensity. As the Dy concentration rises over 3 mol%, the brightness intensity decreases due to quenching phenomena.

Keywords: Phosphors, calcium carbonate, biomimetic synthesis, green synthesis

1. Introduction

Green synthesis refers to synthesizing materials that have environmentally friendly and sustainable. In the case of dysprosium-doped $CaCO_3$, involves a green approach to produce luminescence material. $CaCO_3$ is a commonly found as mineral that has many applications in industry [1]. It can synthesize by using a variety of methods which own toxic chemicals and high temperatures. These methods are not environmentally friendly and also cost effective. In contrast, green synthesis methods use natural sources, such as plant extracts or microorganisms, to synthesize different materials [2]. These methods are generally safer and more sustainable than traditional synthesis methods. Dysprosium-doped $CaCO_3$ is a material that has potential applications in different areas such as catalysis, sensors, and biomedicine. Photoluminescence is the emission of light by a material when it is excited by light of a certain wavelength [3]. Photoluminescence studies provide information about the electronic structure of a material and its potential applications [4]. Here a green approach has developed to synthesize Dysprosium-doped $CaCO_3$ which acting as photoluminescence material by using a plant extract to synthesize the $CaCO_3$ particles [5]. Dysprosium was then incorporated into the $CaCO_3$ particles using a co-precipitation method.

The photoluminescence properties of the material were studied which shows strong photoluminescence in the visible range, with a peak at around 575 nm. This suggests that dysprosium-doped $CaCO_3$ has potential applications in areas such as lighting and displays [6]. Overall, the green synthesis and photoluminescence study of dysprosium-doped CaCO3 demonstrates the potential of using environmentally friendly methods to produce materials with useful properties. The bandgap of $CaCO_3$ polymorphs is broad and straight [7]. After

analyzing its electric, visual, and structural characteristics, the indirect energy gap of $CaCO_3$ was revealed to be 5.07 electron volt. In comparison to other inorganic materials, $CaCO_3$ has shown promising potential for developing effective transporters for a variety of anti-malignant neoplastic medications [8]. $CaCO_3$ is suited for controlled degradability because of these characteristics. Ca^{2+} has been proven to reduce salinity and promote plant growth [9, 10]. The development of effective green methods for the manufacturing of metallic nanoparticles has received a lot of attention in recent years [11]. Plants are one of the most frequently studied methods for digesting metal nanoparticles. The most often used techniques for producing $CaCO_3$ include chemical precipitation, electrochemical, reverse microemulsion methods, hydrothermal synthesis sonochemical precipitation, and chemical reduction [12, 13]. Nevertheless, developing $CaCO_3$-based controlled drug delivery on a massive scale in a rapid and ecologically acceptable manner remains a challenge [14]. Ca is present in over 80 different calcium oxalate forms, including organic matters (lime). $CaCO_3$-based substance used to enhance soil quality in anaerobic conditions by increasing pH and water-holding capability. When applied to the soil, farming lime is made from calcareous materials like sandstone and cement, as well as a variety of other substances, and it works as a calcium supply for plants. Limestone, hematite, and mullite are the three main crystalline calcium phosphate minerals. Calcite is the most prevalent mineral on the planet and has the highest crystallinity under normal conditions [15]. Physical and chemical approaches making calcium carbonate nanoparticles include dispersed phase particles [16]. In recent years, the growth of well-organized methods for the manufacturing of metallic nanoparticles has been a major focus [17]. Even though other researchers have attempted to synthesize Calcium carbonate nano particles using biological pathways in microbes, lengthy is the only one who has succeeded [18]. After that calcite, aragonite is the most abundant $CaCO_3$ form in surface and groundwater ecosystems [19]. High Mg^{2+}/Ca^{2+} ratios in aquatic environments have long been regarded to be helpful for goethite deposition and maintenance. This action has been attributed to dissolved aluminum inhibiting calcium synthesis [20]. Variations in the Mg^{2+}/Ca^{2+} ratio in seawater have been proposed to explain recurrent crystalline shifts in marine $CaCO_3$ bio minerals over Earth's history [21, 22]. Despite mounting evidence that this impact, particularly that of octahedral site oxoanions, is considerable, the involvement of various anions in $CaCO_3$ phase selection has gotten significantly less attention. Furthermore, there is currently no comprehensive examination of near-neutrality conditions. It is difficult to distinguish between both the impacts of acidic and liquid permeability [23]. The effect of additives on carbonate ion crystallization has received a lot of attention, but the technique by which chemicals affect deposition under close circumstances is unknown. $CaCO_3.6H_2O$ is a non-equilibrium calcareous phase with unknown creation techniques. Since the nineteenth century, researchers have developed synthetic $CaCO_3.6H_2O$ [24, 25]. It was discovered in Mother Nature on the bottom of Norway's Ika Fjord and then in marine sediments [26]. Ikaite can be formed in habitats where positive and high PO_4 levels exist. Ikaite, a material with low PO_4 values, was discovered in ice sheets lately [27, 28]. Various experimental settings (pH varying from 8.5 to 10.0 and phosphate concentrations varying from 0 to 50 mol kg at heat and high salinity down to 105 were used in recent research to examine how these factors impact ikaite formation under sea ice conditions. Considering that ikaite is a superfluid Ca salt carbonate, it was discovered to be the only carbonate polymorphism in ice sheets. The $CaPO_4$ polymorphism selection approach influenced by experimental conditions was chosen for this study. Dysprosium-doped materials have sparked a lot of attention due to their white light emission [29]. Dy^{3+} ions produce a large number of emission bands due to their f–f transitions. Dy^{3+} ion visible luminescence consists of a creamy band at 570–600 nm and an azure band at 470–500 nm [30]. With the expansion of protection of the environment and energy-saving consciousness, producing eco-friendly luminaires has become increasingly important. White light emitting diodes (W-LEDs) which are preferable alternatives for ordinary conventional or

neon lamps, have gotten a lot of attention because of their appealing properties, including superb stability, high light efficiency, extended service life, and environmentally friendly nature [31, 32]. In general, white light emitting diodes (W-LEDs) are generated when several phosphors join with diverse emission colors; nevertheless, intestinal absorption in different phosphors diminishes the appliance's performance and productivity in energy loss. As a result, scholarly interest has grown in the study of single- or single-phase white-releasing phosphorus to create blue, green, and red lights that may be combined to make white light. Such phosphorous has progressed to higher rates, such as decreased production costs, improved color depiction, and reduced color aberration [33]. The Dy^{3+} ion has been widely studied as a bright center under white light illumination due to its two distinct emissions at roughly 470 to 500 nm and 560 to 600 nm, which correspond to $^4F_{9/2}$ to $^6H_{15/2}$ and $^4F_{9/26}$ (induced dipole transition), respectively. The host or crystallographic field that surrounds the Dy^{3+} transition has a significant impact on its strength. When compared to a dipolar transition, an induced dipole conversion is generally too sensitive to its surroundings. The yellow light source prevails when Dy^{3+} ions are present in poor symmetry areas without an inversion center. As a result, by altering the strength: (Y/B) among yellow and blue emissions, white light emitted from Dy^{3+} single-doped material may be formed. Dy^{3+} single-doped instances, on the other hand, rarely generate high-quality white light due to the lack of a blue spectral component. To overcome this problem, Dy^{3+} systems sometimes include a second blue light-producing center to compensate for the lack of blue light components. Since its conversion from $^1D_2$ to $^3F_4$ might generate blue waves at 450 nm, the Tm^{3+} ion is a true-blue light absorber. All of the compounds were used just as they were given to us, with no further processing. As per the required stoichiometric fraction, the raw materials were adjusted using a conventional synthesis technique. They were then equally crushed and placed in the close-packed fissures. In a designed muffle furnace, the mixture was then sintered in air for four hours at 1300 degrees centigrade. Finally, the as-prepared energy of the specimens was gathered when the naturally chilled furnace had reached room temperature [34].

2. Materials and methods

2.1. Material required

Host material Calcium Carbonate $CaCO_3$ was prepared by the method of green synthesis. In this preparation, 500g of melon purchased from the market was washed at home and the melon pieces of melon were boiled in 100mL deionized water for 30 minutes for excretion of polysaccharide. Using the chemical balancing formula, the required weights of sodium carbonate (Na_2CO_3) and Calcium Chloride ($CaCl_2$) 5.2994gm and 5.549gm are used in this experiment [35].

2.2. Synthesis Procedure

The green production of $CaCO_3$ phosphors will carried out by extracting $CaCO_3$ from a brine solution of $CaCl_2$ and Na_2CO_3. In the $CaCl_2$, the leaf extracts, which consist of polysaccharides, will be formed by the addition with the help of a syringe or measuring cylinder. For 30 minutes, the specific solution will be heated on a hot plate. After mixing, Na_2CO_3 will added to get the white precipitate and the entire solution will agitated for 30 minutes. At a centrifugation rate of 4000 rpm, the spin machine will segregate these white precipitates. To remove non-reacted calcium carbonate, the white precipitate is frequently washed with distilled water ($CaCO_3$).

2.3. Green synthetic approach of calcium carbonate

Firstly, $CaCO_3$ was obtained from the salt solution of Calcium chloride ($CaCl_2$) and sodium carbonate (Na_2CO_3) by dissolving in 50mL distilled water. Polysaccharides obtained from melon are added in small quantities with the help of a graduated cylinder to calcium chloride solution ($CaCl_2$). The specific solution was stirred on a Hot plate for 90 minutes and then added to Na_2CO_3. The whole solution ($CaCl_2$ containing fruit extract and Na_2CO_3) was stirred further for 30 minutes to obtain the white precipitate. The centrifuge machine separates these white precipitates at the rate of centrifugation 4000 rpm. The white precipitate was washed so often with distilled water to separate non-reacted calcium carbonate ($CaCO_3$). To eliminate unstable components and reduce internal shrinkage,

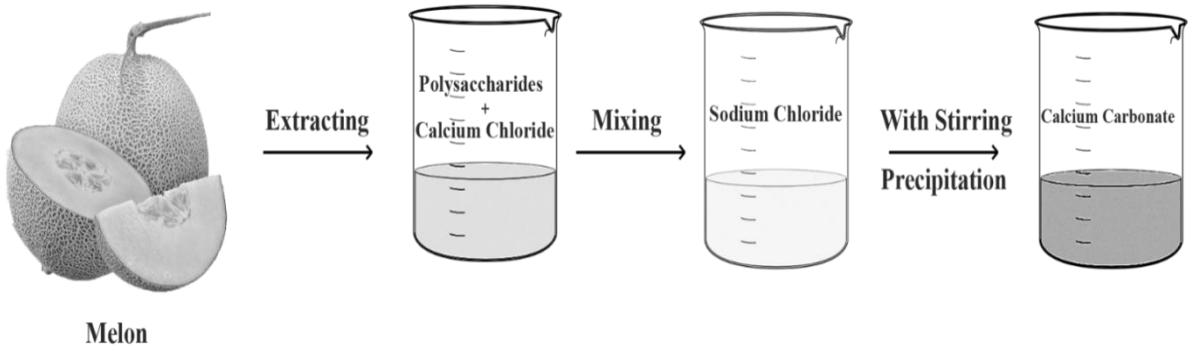

the calcination procedure includes burning the substance in a kiln at a rate of 10° per minute before its transition point.

Figure 1. Schematic diagram of the synthesis of calcium carbonate.

The tiny particles form into medium-sized crystals when a portion of the substance is oxidized [36]. Five samples of pulverized material powder are placed in an oven with a platinum crucible during the sintering process. Figure 2 depicts the sintering furnace used in the method. In the furnace, the material is heated to below the melting temperature, with the temp increasing at a continuous rate of 100 ° C. each hour. The temperature of the material was raised to 550 degrees Celsius before being lowered at a rate of 100 ° C per hour.

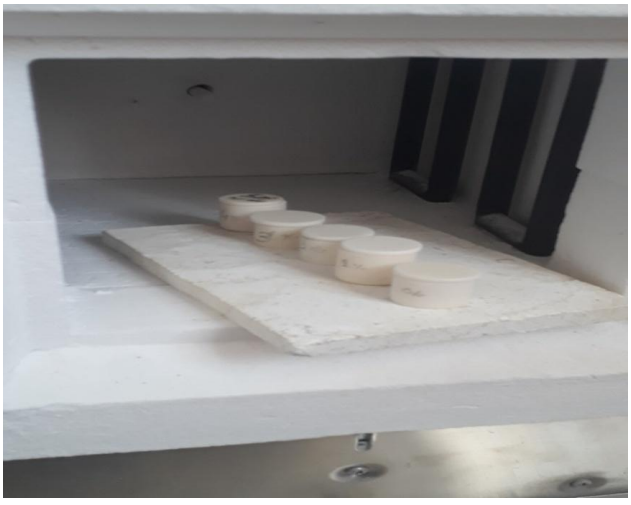

Figure 2. Furnace used for sintering.

2.4. Characterization

At the University of Peshawar's Centralized Resource Laboratories, the uniform geometry, phase clarity, and crystalline nature of the synthesized samples will be evaluated using XRD, SEM, and analysis. UV-Vis spectroscopy and FTIR capabilities will be used to analyze the samples at the MRL, Department of Physics, University of Peshawar. To analyze the surface morphology and grain size of the material, SEM pictures of the undoped $CaCO_3$ phosphor and the Dy^{+3} doped $CaCO_3$ phosphor were acquired. To determine the crystal nature of the material, XRD techniques are used, and the comparison is made to conventional I.C.D.D. No J.C.P.D.S. # 00-047-1743 XRD peaks. To assess the luminous property of the synthesized material, the UV-induced photoluminescence technique is utilized.

3. Results and discussion

The Ca^{2+} ions in $CaCO_3$ have two unique octahedral crystallographic orientations due to their olivine structure. The Ca cation is surrounded by six anions and is located at the center of the version, with an average Ca-O distance of 2.3954 and octahedral coordination. The luminous properties of a Dy^{+3}-based phosphor have been investigated. Dysprosium is an excellent host material for light emitting diode (LED). properties due to its high density. The capacity of Dysprosium to generate unique color bands has piqued people's curiosity. As a result, a Dy-based phosphor gives better light for various bands at varying concentrations of the host. Our substance is a Dy^{+3} doped $CaCO_3$ phosphor. Several methods, like XRD, SEM, and UV photoluminescence, are used to characterize our

product once it has been manufactured utilizing the green synthesis procedure.

3.1 X-ray diffraction

The phases were identified, the structure's crystallinity was measured, and the degree of openness or flaws inside the solid solutions were seen using X-ray diffraction. The diffractometer utilized was a Phillips PW 1800 with a Cooper X-ray tube. At a stress of 40 kV and a current of 20 mA, Cu Ka rays were employed to measure the size. The diffraction spectra were created using a two-step size of 0.02 and improved clarity at an angular rate of 0.008 °/s and a period per step of 0.5 at two angles ranging from 20° to 50°. Peak intensities in X-ray diffraction spectra are expressed as a percentage of the measurement angle 2q. The interplanar defines the level, d, associated with the peaks are determined in a first order using Bragg's diffraction law, n = 2dsinθ by comparing the data gathered from the samples to the X-ray diffraction data for pure substances at the International Center for Diffraction Data, the projected maxima in the diffraction pattern were allocated 15 Miller indices. The study of alloy constituent patterns is based on the notion that each phase develops its own pattern in the absence of other phases. An industrious, strong arrangement is regularly of the interstitial kind, with a synthesis extending from an unadulterated end-part, A, to another unadulterated end-part, B, which ought to both have a similar design [37]. Accordingly, because each of the pieces in such a blend has a similar calculation, their powder stages are practically comparative, with the exemption that arrangement changes to adjust the diffraction-line areas as the crystallite size changes. Terminal arrangements An and B, as meta niobate compounds, are generally just miscible in each other. Whenever A particles are first positioned in B destinations, they structure a strong arrangement, which makes the B grid augment given the relative sizes of the An and B iotas. The grid increments on the off chance that embedding molecule An is more prominent than subbing iota B; assuming it is more limited, the framework contracts [38]. An immersion limit is accomplished because of the reasonable size distinction between the two iotas, and further expansions in a single molecule bring about the precipitation of a third stage, which can be rich A-rich or B-rich, or a temporary stage on the off chance that it isn't related with all things considered. The subsequent material of this center translucent stage is remarkable from either end part's glasslike stage [39]. Figure 3 analyzes the XRD pinnacles of Dy-doped $CaCO_3$ phosphor to the I.C.D.D. Reference No J.C.P.D.S. #00-047-1743 reference information. The pinnacles of our material are the same as those of the reference material, demonstrating the required stage for the created phosphor, which has a Trigonal (Rhombohedral) structure with aspects a=4.315A0, b=4.315A0, and c= 17.061A0 has been met [40]. The places of the XRD tops delivered by the host materials associated with the places of the pinnacles got from our example, with the best pinnacle apparent at 2 = 29.495 from the (104) plane. The XRD estimations and pinnacles show that our material is translucent [41].

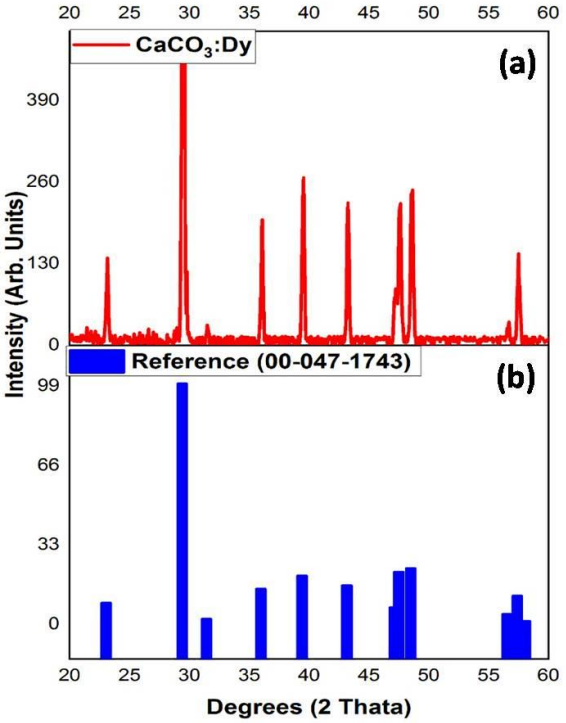

Figure 3. XRD peak comparison of (a) the synthesized sample (Dy-doped CaCO3) with (b) reference material.

3.2 UV Photoluminescence Spectrum

Photoluminescence spectroscopy was performed utilizing V.U.V. excitation, joined by a radio assessment. To create

excitation photons, a Deuterium Lamp - Hamamatsu Model L1835 with proficient outflow from 115 nm to 400 nm was utilized. The light is then coordinated to a round reflect, which focuses the photon stream into the section cut of the vacuum monochromator - A.R.C. Model VM-502. The excitation frequency was resolved utilizing a 1200 G/mm grinding covered with Iridium, permitting it to be used in the far-off U.V. area of an electromagnetic range. The entire range is accomplished by light falling on the grinding as a point load from the vacuum monochromator's entrance cut. The grinding is turned to decide the frequency utilizing an A.R.C. Spectra Drive Model 748 work area with Lab View drivers. From that point forward, photons of a particular frequency are centered around the example apportionments advisory group section cut. A Turbodyne siphon was utilized to vacuum the circular mirror confine, test holder, and monochromator/grinding. The photoelectrochemical emission exits the specimen chamber in a wide beam, which collimates and concentrating optics contain and route to the spectrometer. The focused light is then passed through a filter that keeps frequencies shorter than 335 nm from entering the measuring equipment. Figure 4 portrays the photoelectrochemical spectra of Dy-doped $CaCO_3$ materials as well as $CaCO_3$ PL spectra at around 350nm [42]. The emanation spectra of Dy-doped $CaCO_3$ phosphor are extremely indistinguishable from that of Dy-doped $CaSrAl_2SiO_7:Dy^{3+}$ phosphor. Figure 4 shows a few lines for Dy-doped $CaCO_3$, with the most noteworthy pinnacle happening at 578nm. A comparable pinnacle is noticed for $CaSrAl_2SiO_7:Dy^{3+}$doped with Dy [43]. The 483 nm tops produced by Dy-doped $CaCO_3$ are entirely practically identical to those created by Dy-doped $CaSrAl_2SiO_7:Dy^{3+}$phosphor. The changeover from the $^4F_{9/2}$ to the $^6H1_{5/2}$, the two of which produce blue light, causes this zenith. As an outcome, Dy-doped phosphor can be utilized as a phosphor with a blue-to-yellow tone [41].

3.3. $CaCO_3$ phosphor photoluminescence spectrum with varies concentration of dysprosium

Figures 5 represent photoluminescence spectra with expanding levels of doped Dy for $CaCO_3$ phosphor. At Dy groupings of 1, 2, 3, and 4 mol percent, the power is shown. $CaCO_3$ phosphor emanates enlightenment up to 4 mol% Dy focus. Figure 4 shows the best power with a Dy level of 3 mol. Our example's extinguishing bend reflects that of impacted with changing Dy fixations [44]. A 2% mol percent of Dy doped $CaSrAl_2SiO_7:Dy^{3+}$ Phosphor works on the force. In view of the confined number of radiances focuses, the luminance is initially fairly low in the two examples. Since there are a critical number of glow foci at these fixations, the best iridescence is found at 3 mol % for $CaCO_3$ phosphor. Figure 5 shows that the pinnacle power happens at a frequency of 578nm, finishing in yellow light [45]. Thus, the centralization of 3 mol % Dy is picked above different fixations.

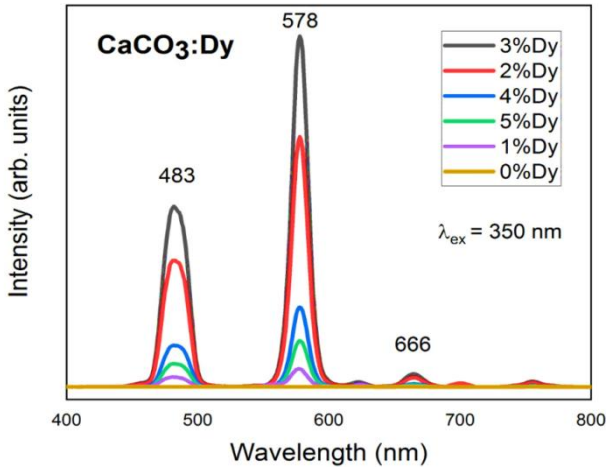

Figure 4. Dy doped $CaCO_3$ excitation spectrum.

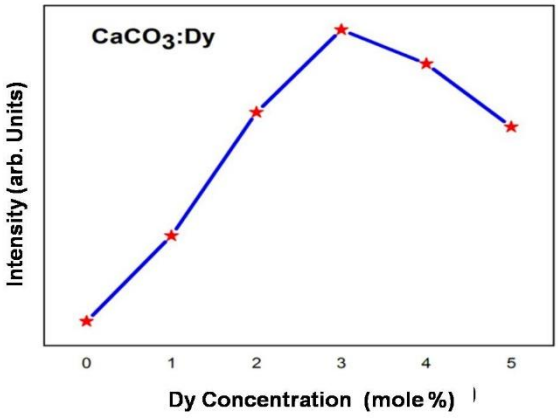

Figure 5. $CaCO_3$ phosphor quenching curve with varying Dy concentrations.

3.4. Scanning electron microscopy

Figures 6(a), 6(b), 6(c), 6(d), and 6(e) show SEM micrographs of pure CaCO3 phosphor with 0%, 1%, 2%, 3%, and 4% concentration Dysprosium added, respectively.

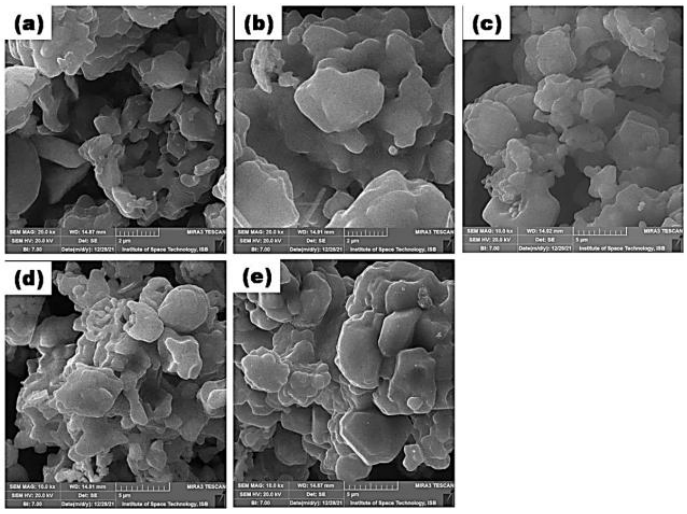

Figure 6. SEM images (a) $CaCO_3$:0% (b) $CaCO_3$:1% (C) $CaCO_3$:2% (d) $CaCO_3$:3% (e) $CaCO_3$:4%.

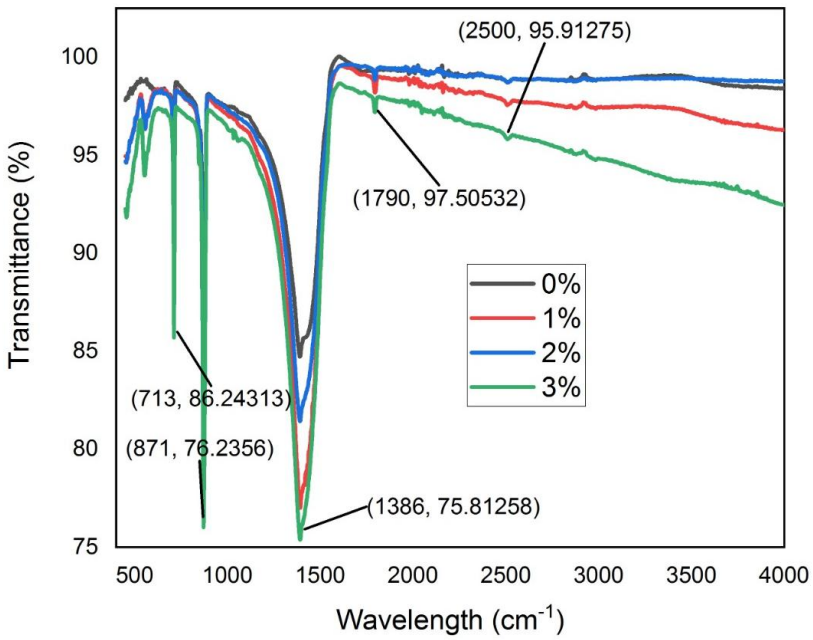

Figure 7. FTIR Spectra of Dy doped $CaCO_3$

The particle shape and size are not the same for everyone, but they are uniformly distributed across the surface. In the snapshot, we can observe tiny and big particles of various sizes and shapes. These images validate the material's microstructure, which is essential for luminescence [46, 47]. The grain is 1 to 20 micrometers in diameter because the typical particle size collects radiation effectively and emits it from the surface. As a result, the brightness improves. The photos clearly illustrate that particle size has a little tendency to grow as the number of dopants rises.

3.3. Fourier transforms infrared spectroscop

The FTIR spectra of Dy doped $CaCO_3$ are found in Figure 7. The $CaCO_3$ FTIR investigation tops for CO_3 particles because of vibration tops v1 symmetric extending and 3 deviated vibration [47]. Carbonate CO_3-topsy-turvy twisting vibrations causes the tops at (1386,75.81258) cm^{-1}, (871,76.2356) cm^{-1}, and (1790,97.50532) cm^{-1}. The realism obviously shows that as the convergence of doping increments, so does the strength of the pinnacles. The biggest pinnacles were found at (1386, 75.81258) cm^{-1} 3-mol% dysprosium.

4. Conclusion

Granular samples of $CaCO_3$ doped with 0%, 1%, 2%, 3%, and 4% of Dy^{3+} were generated using a standard solid-state synthesis technique. According to XRD results, the pure phase was achieved after three hours of heating at 550 Celsius for all dopant concentrations. In the range of 300 to 500 nm, the Dy^{3+} excitation spectrum exhibits characteristic Dy^{3+} transitions, with the strongest peak at nm (6H15/2 6P7/2 transition). In the luminescent spectra in the range of 400 to 650 nm, Dy^{3+} emission peaks appear at 483 nm (4F5/26H15/2 transition) and 578 nm (4F5/26H13/2 transition), corresponding to blue and yellow. The highest emission is observed at 3mol percent Dy^{3+} dopant concentrations. Samples with varying Dy^{3+} concentrations had yellow-to-blue (Y/B) intensity ratios ranging from 1 to 3. Changing the concentration of active ions can change the color to some extent. The C.I.E. coordinates of the samples in the yellow zone exhibit a variety of emission colors. The findings indicate that the dysprosium-doped materials can be used as yellow phosphors.

Authors Contribution

Majid Ali and Muhammad Jamshed conceptualized the study, supervised the research, and contributed to the design of the methodology and manuscript revisions. Muhammad Bilal, Hammad Haider, Salman Ahmad, and Saeed Anwar participated in data collection, data analysis, and drafting the manuscript. All authors reviewed and approved the final version of the manuscript. Majid Ali and Muhammad Jamshed served as corresponding authors and ensured the overall quality and completion of the work.

Conflicts of Interest

There is no conflict of interest between the authors.

Acknowledgment

The authors are thankful to the Department of Chemistry, Kohat University of Science and Technology, Kohat-26000-Khyber Pakhtunkhwa, Pakistan, for financial support.

Data Availability statement

The data presented in this study are available on request from the corresponding authors.

Funding

Not applicable

REFERENCES

1. Behera, M., et al., Fabrication of energy efficient PiG structure with novel dysprosium-doped yttrium calcium borate (Dy: Y2CaB10O19) phosphors: Highly efficient materials for cool white light emission conducive to green technology. Dyes and Pigments, 2024. 22: p. 112-225.
2. Rathod, S., et al., Exploring synthesis and applications of green nanoparticles and the role of nanotechnology in wastewater treatment. Biotechnology Reports, 2024. 3(9): p. 08-30.
3. Neacsu, I.A., et al., Luminescent hydroxyapatite doped with rare earth elements for biomedical applications. Nanomaterials, 2019. 9(2): p. 239.
4. Martinez, F.M., Luminescent Hydroxyapatite: Degradation Study and Osteogenic Potential. 2024. 2(4): p. 812-244.
5. Adeleye, S.O., et al., A Review of the Physical, Optical and Photoluminescence Properties of Rare Earth Ions Doped Glasses. Trends in Sciences, 2024. 21(12): p. 8759-8759.
6. Pangul, C.N., S.W. Anwane, and S.B. Kondawar, Enhanced photoluminescence properties of electrospun Dy3+-doped ZnO nanofibres for white lighting devices. Luminescence, 2018. 33(6): p. 1087-1093.

7. Misevičius, M., Synthesis, structural characterization and optical properties of selected strontium aluminates. Luminoius matirals, 2016. 39(4): p.481-492.
8. Hossain, F.M., et al., Electronic, optical and bonding properties of CaCO3 calcite. Solid state communications, 2009. 149(29-30): p. 1201-1203.
9. Yao, C., et al., Green synthesis of calcium carbonate with unusual morphologies in the presence of fruit extracts. Journal of the Chilean Chemical Society, 2013. 58(4): p. 2235-2238.
10. Savithramma, N., Influence of calcium supply on biomass production of endemic and endangered tree species of Tirumala hills of South Eastern Ghats. J. Indian Bot. Soc, 2002. 81: p. 323-326.
11. Guo, Y., et al., Facile green synthesis of calcium carbonate/folate porous hollow spheres for the targeted pH-responsive release of anticancer drugs. Journal of Materials Chemistry B, 2016. 4(34): p. 5650-5653.
12. Chen, S.-F., et al., Ethanol assisted synthesis of pure and stable amorphous calcium carbonate nanoparticles. Chemical Communications, 2013. 49(83): p. 9564-9566.
13. Khan, M., et al., Supramolecular solvent–based liquid phase extraction of antimony prior to spectrophotometric quantification. Environmental Monitoring and Assessment, 2022. 194(8): p. 591.
14. Gupta, R., Synthesis of precipitated calcium carbonate nanoparticles using modified emulsion membranes. Matirals, 2004. 200(6): p.751-762.
15. Yang, T., et al., Biomineralization inspired synthesis of CaCO3-based DDS for pH-responsive release of anticancer drug. Materials Today Communications, 2021. 27: p. 102256.
16. Reddy, A. and N. Savithramma, Effect of calcium chloride on growth and biochemical changes of black gram (Vigna mungo) under salt stress. Golden Research Thoughts, 2013. 3(2): p. 1-6.
17. Piskin, S. and O. Ozdemir, Effect of process conditions on crystal structure of precipitated calcium carbonate (CaCO3) from fly ash: Na2CO3 preparation conditions. Int. J. Biol. Ecol. Environ. Sci, 2012. 1(6): p. 2277-4394.
18. Sadowski, Z., I. Polowczyk, and A. Frackowiak, Bioinspired synthesis of calcium carbonate colloid particles. Collides and Interfacese, 2010. 17: p. 215-122.
19. Hu, Z., Y. Deng, and Q. Sun, Synthesis of precipitated calcium carbonate nanoparticles using a two-membrane system. Colloid Journal, 2004. 66: p. 745-750.
20. Ankanna, S., et al., Production of biogenic silver nanoparticles using Boswellia ovalifoliolata stem bark. Dig J Nanomater Biostruct, 2010. 5(2): p. 369-372.
21. Grasby, S.E., Naturally precipitating vaterite (μ-CaCO3) spheres: unusual carbonates formed in an extreme environment. Geochimica et Cosmochimica Acta, 2003. 67(9): p. 1659-1666.
22. Radha, A., et al., Transformation and crystallization energetics of synthetic and biogenic amorphous calcium carbonate. Proceedings of the National Academy of Sciences, 2010. 107(38): p. 16438-16443.
23. Gebauer, D., A. Volkel, and H. Colfen, Stable prenucleation calcium carbonate clusters. Science, 2008. 322(5909): p. 1819-1822.
24. Falini, G., M. Gazzano, and A. Ripamonti, Crystallization of calcium carbonate in presence of magnesium and polyelectrolytes. Journal of Crystal Growth, 1994. 137(3-4): p. 577-584.
25. Song, R. Q. and H. Cölfen, Additive controlled crystallization. Cryst Eng Comm, 2011. 13(5): p. 1249-1276.
26. Hoch, E., Earth science as a philosophical background to medicine: an essay based on the autobiography of Dr Otto Sperling (1602–81). Geological Society, London, Special Publications, 2017. 452(1): p. 9-33.

27. Pelouze, M., Sur une combinaison nouvelle d'eau et de carbonate de chaux. Chemical Review, 1865. 60: p. 429-431.
28. Suess, E., et al., Calcium carbonate hexahydrate from organic-rich sediments of the Antarctic shelf: precursors of glendonites. Science, 1982. 216(4550): p. 1128-1131.
29. Dieckmann, G., et al., Brief communication: Ikaite (CaCO 3· 6H 2 O) discovered in Arctic sea ice. The Cryosphere, 2010. 4(2): p. 227-230.
30. Gu, F., et al., Combustion synthesis and luminescence properties of Dy3+-doped MgO nanocrystals. Journal of Crystal Growth, 2004. 260(3-4): p. 507-510.
31. Gu, F., et al., Structure evaluation and highly enhanced luminescence of Dy3+-doped ZnO nanocrystals by Li+ doping via combustion method. Langmuir, 2004. 20(9): p. 3528-3531.
32. Huang, D., et al., Photoluminescence properties of M3+ (M3+= Bi3+, Sm3+) activated Na5Eu (WO4) 4 red-emitting phosphors for white LEDs. Journal of alloys and compounds, 2013. 554: p. 312-318.
33. Geng, W., et al., NaBaY (BO3) 2: Ce3+, Tb3+: A novel sharp green-emitting phosphor used for WLED and FEDs. Journal of the American Ceramic Society, 2018. 101(10): p. 4560-4571.
34. Li, K., et al., Photoluminescence properties of single-component white-emitting Ca 9 Bi (PO 4) 7: Ce 3+, Tb 3+, Mn 2+ phosphors for UV LEDs. Journal of Materials Chemistry C, 2015. 3(27): p. 7096-7104.
35. Patnam, H., et al., Near-ultraviolet excited Tm3+ and Dy3+ ions co-doped barium lanthanum silica oxide phosphors for white-light applications. Journal of Alloys and Compounds, 2019. 780: p. 846-855.
36. Ahmadi, S., et al., Prebiotics from acorn and sago prevent high-fat-diet-induced insulin resistance via microbiome–gut–brain axis modulation. The Journal of nutritional biochemistry, 2019. 67: p. 1-13.
37. Mohamed, W., et al., Effect of heavy Dy3+ doping on the magnetic, structural, morphological, and optical characteristics of CuDyxFe2-xO4 nanoparticles. Ceramics International, 2024. 15: p. 22-42.
38. Lakshmanan, A., et al., Application of microdosimetric concepts in CaCO3: Ce3+/Dy3+ for megalevel radiation dosimetry. Nuclear Instruments and Methods in Physics Research Section B: Beam Interactions with Materials and Atoms, 2021. 487: p. 12-24.
39. Ramasamy, V., et al., A novel and simple approach of rare earth ions (Y3+ and La3+) decorated nano calcium carbonate/polyethylene glycol for photocatalytic degradation of organic pollutants in wastewater. Optical Materials, 2023. 142: p. 114130.
40. Jung, S.-Y., et al., Tannylated calcium carbonate materials with antacid, anti-inflammatory, and antioxidant effects. International Journal of Molecular Sciences, 2021. 22(9): p. 4614.
41. Kandiah, K.K., et al., Study on photoluminescence of integrated nano-calcium carbonate (CaCO3) enhanced with dysprosium (Dy) doped calcium borophosphate (CBP) phosphor. Pigment & Resin Technology, 2023. 46(400): p. 200-212.
42. Venugopal, A., et al., Dy3+ doped B2O3–Li2O–CaO–CaF2 glass for efficient white light emitting sources. Journal of Non-Crystalline Solids, 2021. 554: p. 120604.
43. Dong, Y., et al., Preparation and tunable luminescence of CaCO 3: Eu 3+, Dy 3+ phosphors. Functional Materials Letters, 2014. 7(04): p. 1450038.
44. Rai, S., et al., Neutralization and utilization of red mud for its better waste management. World, 2012. 6: p. 5410.
45. Harries, M.E., Vapor-liquid Equilibria Pertaining to the Study of Alternative Fuels and the Forensic Analysis of Chemical Evidence. University of Colorado at Boulder, 2018. 44: p. 15-22.
46. Ayoub, I., et al., Structural, optical, and color-tunable luminescence of Dy3+-doped Ca3Ga4O9 phosphors

for white-light emitting diode applications. Materials Science and Engineering: B, 2024. 310: p. 117724.

47. Venkidasamy, R., et al., Synthesis of CaCO3 nanocomposite from natural carbonate source and its effect on the inclusion of Eu3+ ions for photocatalytic activity. Chemical Engineering Communications, 2024. 211(2): p. 229-250.

How to cite this article:
Bilal, M., Ali, M., Haider, H., Ahmad, S., Anwar, S., Jamshed, M. (2024). Green synthesis and photoluminescence study of Dy-doped $CaCO_3$. *Journal of Chemistry and Environment,* 3(2), 58-67.